Journal of King Saud University – Science 34 (2022) 101879

Contents lists available at ScienceDirect

Journal of King Saud University – Science

journal homepage: www.sciencedirect.com

Original article

Polyvinyl alcohol/corn starch/castor oil hydrogel films, loaded with silver nanoparticles biosynthesized in *Mentha piperita* leaves' extract

Mariam Mojally [a], Eram Sharmin [a,*], Najla A. Obaid [b], Yosra Alhindi [c], Ashraf N. Abdalla [d]

[a] Department of Pharmaceutical Chemistry, College of Pharmacy, Umm Al-Qura University, Makkah 21955, Saudi Arabia
[b] Department of Pharmaceutics, College of Pharmacy, Umm Al-Qura University, Makkah 21955, Saudi Arabia
[c] Department of Pharmacology and Toxicology, College of Medicine, Umm Al-Qura University, Makkah 21955, Saudi Arabia
[d] Department of Pharmacology and Toxicology, College of Pharmacy, Umm Al-Qura University, Makkah 715, Saudi Arabia

ARTICLE INFO

Article history:
Received 29 October 2021
Revised 15 January 2022
Accepted 27 January 2022
Available online 2 February 2022

Keywords:
PVA
Starch
Hydrogels
Wounds
SEM
Antibacterial

ABSTRACT

Objectives: Hydrogel films were prepared from Polyvinyl alcohol [PVA], Corn starch [CS], Castor oil [CO] and silver nanoparticles [SNP], biosynthesized in leaves' extract of locally grown *Mentha piperita* L. (Family, Labiatae) for prospective application as wound dressings.
Methods: Both aqueous [AME] and methanolic [MME] extracts of *Mentha piperita* leaves were used for phytochemical synthesis of SNP, that were later dispersed in hydrogel matrix by simple blending of the constituents (PVA, CS, CO, AME/MME and SNP) and crosslinking with glutaraldehyde.
Results: The hydrogel films were flexible and biodegradable. The structure analysis by FTIR suggested hydrogen bonding between the functional groups of PVA, CS and CO in the films. SEM analysis revealed that SNP globules were distributed (10.02% and 12.57%) throughout the hydrogel matrices that were prepared from both AME and MME, respectively. The hydrogel films with MME showed higher thermal stability than those formed from AME due to uniform dispersion of small (size $\leq$70 nm) and unagglomerated SNP in the former. The hydrogel films can be safely used upto 200°C. The antibacterial studies exhibited that the films inhibited the growth of both *S. aureus* and *P. aeruginosa*, as investigated by disc diffusion method.
Conclusion: The hydrogel films were prepared through ecofriendly and benign route, devoid of any toxic solvents, diluents, surfactants, stabilizers and can be employed as thermally stable, antibacterial and biodegradable films. The hydrogel films with MME showed better performance than AME films, for prospective application as wound dressings.

1. Introduction

Mentha piperita L. (Family, Labiatae) is one of the important plants in pharmaceutical industry with specific pharmaceutical characteristics. Mentha oil and its extract have antifungal activities against several microorganisms such as *Pseudomonas*, *Aspergillus Niger* and *Fusarium*. Mentha extracts can be defined as primary antioxidants which can prevent the beginning and proliferation of free radical-mediated chain reaction. Therefore, the extract can prevent the oxidative damage on skin (Robles-Martínez et al., 2020; Siddeeg et al., 2018). In addition, Mentha essential oil can be used as potential source of natural antimicrobial agents (Narayanan and Sakthivel, 2010; Rajeshkumar et al., 1872).

Metal nanoparticles have specific and unique physical, biological and chemical properties that have gained the attention of researchers in the past decades. They are used in diverse areas, for example, beauty care products, drug delivery and coatings (Ghosal et al., 2019; Ghosal et al., 2015). Silver, gold and platinum nanoparticles have been used in cosmetics and pharmaceutical products. In addition, some other known metal nanoparticles including zinc, iron, copper and selenium have been successfully used as antimicrobials in medical treatments. Biosynthesis of nanoparticles further augments their significance and applications. Using biological agents such as plant extracts in nanoparticles syn-

* Corresponding author.
E-mail addresses: mamojally@uqu.edu.sa (M. Mojally), esfarooque@uqu.edu.sa (E. Sharmin), naobaid@uqu.edu.sa (N.A. Obaid), yzhindi@uqu.edu.sa (Y. Alhindi), anabdrabo@uqu.edu.sa (A.N. Abdalla).
Peer review under responsibility of King Saud University.

Production and hosting by Elsevier

https://doi.org/10.1016/j.jksus.2022.101879

thesis has become an excellent alternative to traditional methods as it is nontoxic, eco-friendly, clean and inexpensive method. (Mubarak et al., 1873, Narayanan and Sakthivel, 2010; Narayanan and Sakthivel, 2011; Patil and Kim, 2017; Rosman et al., 2020).

Hydrogels have some specific characteristics such as hydrophilicity, biodegradability and biocompatibility that render them suitable for biomedical applications including drug delivery, tissue engineering and wound dressings (Kouser et al., 2018a; Kouser et al., 2018b; Kouser et al., 2018c; Vashist et al., 2019; Vashist et al., 2012; Vashist et al., 2016; Vashist et al., 2012; Vashist et al., 2013; Vashist et al., 2014). The hydrogel films to be used as wound dressings must be non-toxic, biodegradable, antimicrobial to prevent wound infection, with the ability to absorb wound exudates, and control moist environment. PVA and starch blend films have shown good water absorption, film forming behavior and mechanical strength (Hassan et al., 2018; Khan et al., 2021; Sin et al., 2013; Velgosova et al., 2021). CO has been used as antibacterial agent in hydrogels, for skin tissue augmentation, as polyurethane membranes for wound dressing applications, and as multifunctional reagent (Díez-Pascual and Díez-Vicente, 2015; Gharibi et al., 2021; Ghosal et al., 2013; Muzammil et al., 2021; Rezaei Hosseinabadi et al., 2020). In the present research, nanocomposite hydrogel films [PVA:CS:CO] have been fabricated using PVA, CS, and CO, by blending. The latter has been a simple applied technique for preparing hydrogel films (Iqbal et al., 2020). PVA:CS:CO [H] matrix was further loaded with biosynthesized SNP and crosslinked using glutaraldehyde [GA] which favors intermolecular reaction with PVA under mild conditions (Figueiredo et al., 2009).

The proposed research aims (i) to utilize the potential of locally available *Mentha piperita* plant in the biosynthesis of SNP, (ii) to develop transparent and biodegradable nanocomposite hydrogel films using non-toxic components, loaded with biosynthesized nanoparticles, as herbal dressing for wounds, (iii) through environment friendly protocol. The manuscript highlights the properties of hydrogel films obtained from the combination of PVA/CS/CO/mint extract and biosynthesized SNP. The literature review revealed that no research work has been accomplished on such hydrogel films as developed in the present research.

2. Materials and methods

2.1. Materials

CS ($C_6H_{10}O_5$)n, MW (162.14)n (Holyland, Saudi Arabia), PVA, MW 140,000 (HIMEDIA, Mumbai, India), Silver nitrate [SV] (extra pure from ScharlauChemie S.A., Sentmenat, Spain), CO (Loba Chemie, Mumbai, India), Glycerol [GL] (Sigma-Aldrich, Germany), Tween 80 [TW] (Sigma-Aldrich, Germany), GA (Loba Chemie, Mumbai, India) and ethanol (AnalaR NORMAPUR, France), were used as received. Deionized water (DIW) was used in the preparation of hydrogels.

Fresh mint plant *Mentha piperita* (Family: Lamiaceae), was obtained from Alahmadi farm in Madina Al- Monawwarah, Saudi Arabia, in the month of December, and identified by Dr. Kadry Abdel Khalik, Botany Department, Faculty of Applied Sciences, Umm Al-Qura University.

2.2. Methods

2.2.1. Preparation of aqueous mint extract [AME] and methanolic mint extract [MME]

Fresh mint leaves were washed with DIW and dried on the top of the lab bench until no residual water was found on leaves. The leaves were then patted dry again and used to prepare AME and MME.

The leaves were added to boiling DIW (10%w/v) and left covered to boil for 5 min. Next, the extract was cooled slowly to room temperature and filtered through whatmann filter paper to obtain AME.

For preparing MME, the leaves were placed in methanol (25%w/v), left for 24 h at room temperature, and then filtered to obtain MME.

Both AME and MME were stored in dark bottles for future use, if required.

2.2.2. Preparation of silver nanoparticles in aqueous mint extract [SAME] and methanolic mint extract [SMME]

1 ml of AME was added to 9 ml of 0.1 M SV solution. The mixture was placed in dark, at room temperature, for 2 h. Similarly, 1 ml of MME was added to 9 ml of 0.1 M SV solution and placed in dark for 2 h. In both cases, the change in color was observed from green to dark brown. The formation of SNP in AME and MME was confirmed by UV and TEM analysis. The solutions SNP in AME and SNP in MME are termed as SAME and SMME, respectively.

2.2.3. Preparation of hydrogel films

To CS (2.8 g) and PVA (1.2 g) was added DIW (40 ml), CO (0.4 g) and TW (0.4 g), each separately dissolved in ethanol (4 ml) and GL (2 ml) dissolved in ethanol (10 ml). The contents were constantly stirred for 10 min at 80 ± 5 ℃ and then cooled to room tempera-

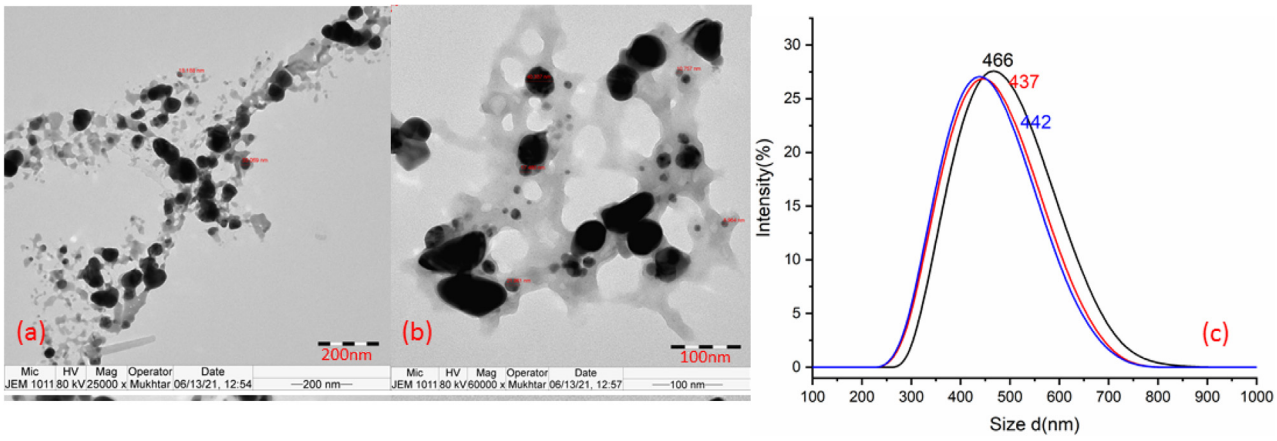

Fig. 1. TEM of SAME.

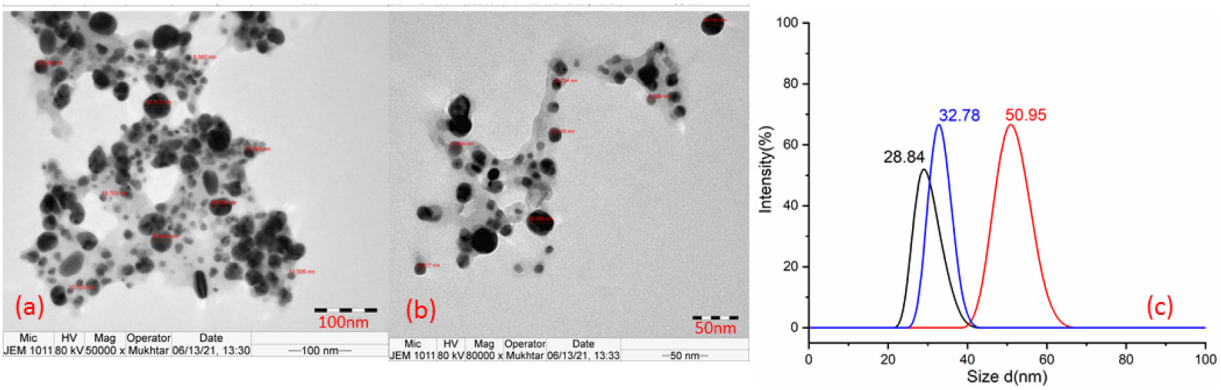

Fig. 2. TEM of SMME.

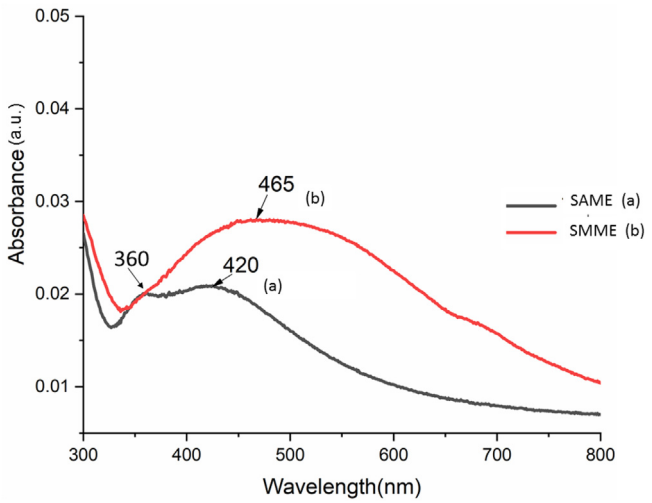

Fig. 3. UV spectra of SAME and SMME.

ture, followed by the addition of SAME, and continuous stirring for 1 h at room temperature. Acidified GA dissolved in ethanol (1 ml) was dropwise added to SAME and PVA:CS:CO blend. The mixture was divided in two portions, each portion was gently poured on a glass petri dish and left to dry at room temperature to produce hydrogel film termed as H-SAME, i.e., hydrogel film (H) developed with SNP biosynthesized in aqueous mint extract. Similar procedure was followed to prepare H-SMME, i.e., hydrogel film developed with SNP biosynthesized in methanolic mint extract.

By similar method, PVA:CS:CO, PVA:CS:CO-AME and PVA:CS:CO-MME hydrogel films were also prepared termed as H, H-AME and H-MME films, respectively.

2.3. Characterization

2.3.1. Spectral analysis, morphology, thermal stability and biodegradation assessment:

FTIR spectra of H, H-AME, H-MME, H-SAME and H-SMME were recorded on FTIR spectrophotometer (Spectrum 100, Perkin Elmer Cetus Instrument, Norwalk, CT, USA) to identify different functional groups. The composition and morphology of films were observed by FE-SEM (JSM 7600F JEOL, Japan) and EDX (Oxford) attached to the SEM instrument. Sample was sputter coated with Pt prior to observation under the microscope and the microscope was operated at 15 kV. The particle size distribution of SNP were determined using Dynamic Light Scattering (DLS) analyzer (Zetasizer Nano, ZSP) Malvern Instruments Ltd., U.K.) and UV analysis was performed on a UV–vis spectrophotometer (Lambda 35) Perkin 202 Elmer lambda, Waltham, MA, USA. TEM analysis was performed on a Transmission electron microscope (TEM)(JEM-2100F) JEOL, Japan, to find out the size and shape of nanoparticles.

Thermal analysis of nanocomposites was carried out by TGA (Mettler Toledo AG, Analytical CH-8603, Schwerzenbach, Switzerland) in nitrogen atmosphere and at heating rate 10°C/min to assess the thermal stability of hydrogel films.

Biodegradation assessment was performed by soil burial method. Hydrogel films were cut in (2 cm × 2 cm) square films. These films were separately buried in soil at the depth of 10 cm. For identification of each sample, a flag with the film code of a particular film was planted over the burial site of that film. The films were carefully pulled out from the soil, after every 4 days, to record the degradation effect of soil, i.e., change in color, texture, weight and overall appearance of the film, and were again replaced at their site and buried, until major changes were observed.

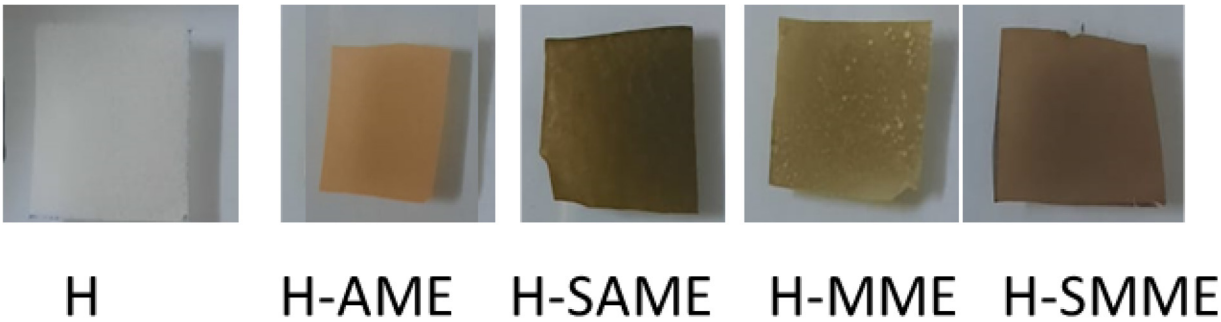

Fig. 4. Hydrogel films of H, H-AME, H-SME, H-SAME and H-SMME.

2.3.2. In-vitro antibacterial test

2.3.2.1. Bacterial isolates. Standard strains (*Staphylococcus aureus* ATCC and *Pseudomonas aeruginosa* ATCC) were sub-cultured from stored frozen (-20 °C) tubes contain glycerol on blood agar purchased from Saudi Prepared Media Laboratory Company Ltd. (SPML Ltd. Dammam) and incubated for 18 h at 37 °C. After the incubation, 3–5 single colonies were inoculated into Nutrient broth media (SPML Ltd. Dammam) and incubated for another 18 h at 37 °C to make a suspension for each strain. These suspensions were standardized at 600 nm optical density equal to 0.1 MacFarland to assure the inoculum prepared with the same number of cells. Then we used disc diffusion method which was adopted according to the Clinical and Laboratory Standards Institute for antimicrobial susceptibility (CLSI, 2010).

2.3.2.2. Preparation of the sample. Each bacterial suspension was added by transferring 100 μl of each standardized suspension then spread on pre-prepared Muller-Hinton agar media (SPML Ltd. Dammam). Two sets of discs were prepared. In the first set, the filter paper discs (6 mm diameter, 0.9 mm thick) were impregnated with CO, AME, MME, SAME and SMME. Then by using sterile forceps, these discs were applied onto the surface of the prepared Muller-Hinton agar media. In the second set, the hydrogel films, H, H-AME, H-SAME, H-MME, H-SMME, were cut into discs (6 mm diameter and 0.9 mm thick). Here, plain hydrogel film H was used as a negative control. One disc of antibiotic (Amoxicillin for *S. aureus* and Amikacin for *P. aeruginosa*) was added in each plate as a positive control. The plates were incubated for 24 h at 37 °C, then the zone of inhibition for each preparation was measured using metric scale.

3. Results and discussion

3.1. Synthesis

Biosynthesis of SNP in mint extract was performed utilizing the phytochemical reduction potential of AME and MME (Khatoon et al., 2018; Robles-Martínez et al., 2020) without using any solvent, surfactant, stabilizer, and capping agent. TEM analysis (Fig. 1) of SAME revealed the presence of large globules of SNP with size ≤ 800 nm, and average particle size as 448 nm. SMME (Fig. 2) showed the presence of spherical SNP of size ≤ 70 nm, with average particle size about 37.5 nm. UV spectrum showed broad peaks with maximum absorption at 420 nm and 465 nm, in SAME and SMME, respectively (Fig. 3). In SAME, an additional peak was observed at 360 nm.

The hydrogel matrix was prepared from CS, PVA, CO, TW and GL. The raw materials used are eco-friendly, and the solvents employed in synthesis are water and ethanol. The nanocomposite hydrogel films were obtained by reinforcing the matrix with SNP biosynthesized in mint leaves' extract: AME and MME(Alam et al., 2020; Sharmin et al., 2021; Sharmin et al., 2020). The crosslinking was carried out by GA. The films were dried at room temperature for 72 h and could be peeled off the glass petridish easily. The hydrogel films prepared were flexible/foldable, crack-free and bubble-free (Fig. 4). The synthesis strategy complies with "greener synthesis" protocol as (i) no reducing or stabilizing agents or diluents were used, (ii) no side reactions occurred, (iii) the preparation of films was carried out at room temperature and, (iv) the hydrogel films were biodegradable.

3.2. FTIR

FTIR spectrum of CO (not shown here) presented absorption bands for- OH (3400 cm^{-1}), -C=C-Hstr (3007 cm^{-1}),–CH_2, CH_3 (2926 cm^{-1} and 2855 cm^{-1}; assym and sym str str), -C=Oester (1740 cm^{-1}), -(CC(=O) -O) (1240 cm^{-1}, 1165 cm^{-1}), –O- C- C -str

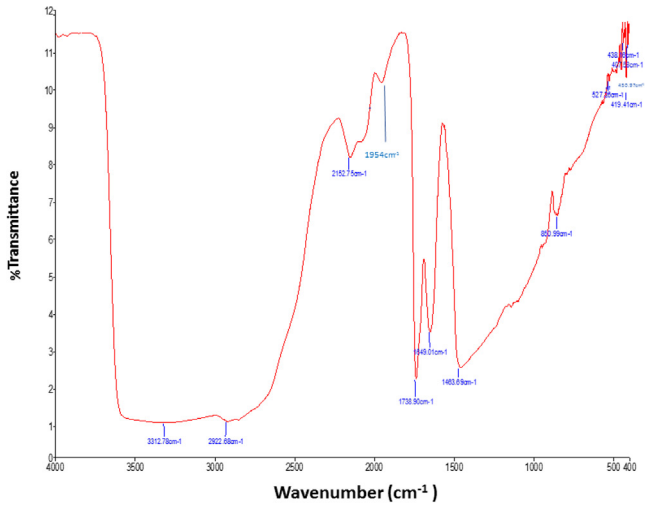

(a) FTIR of H

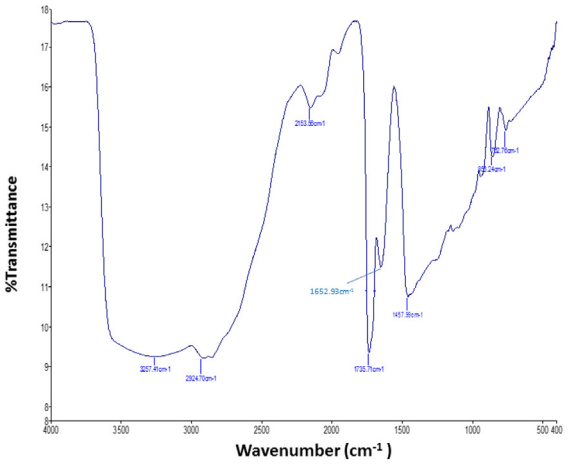

(b) FTIR of H-SAME

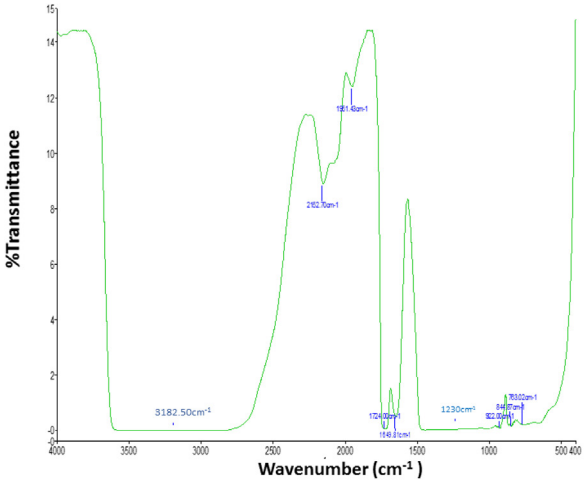

(c) FTIR of H-SMME

Fig. 5. FTIR spectra of H (a), H-SAME (b) and H-SMME (c).

ester (1097 cm^{-1}), C=C (1650 cm^{-1}) and $-CH_3$ (1400 cm^{-1}; bending) (Akram et al., 2008). FTIR spectrum of H, H-SAME and H-SMME (Fig. 5) showed absorption bands at 3000–3600 cm^{-1} (OH), 2800–2900 cm^{-1} ($-CH_2$, $-CH_3$ str), 1738 cm^{-1} (-C=O), 1649 cm^{-1} (-C=C-str), 1300–1400 cm^{-1} (–CH- bending). These were the absorption bands typical for the functional groups present in PVA, CS and CO (Aktürk et al., 2019; Sharmin et al., 2020). However, in all these spectra, the absorption bands were very broad due to inter and intramolecular hydrogen bonding typically between the hydroxyl functional groups of PVA, CS and CO (Tanwar et al., 2021; Vashist et al., 2012; Vashist, Shahabuddin, et al., 2012).

3.3. SEM

SEM micrographs of H, H-AME, H-MME (supporting file a,b,c), H-SAME and H-SMME (Fig. 6) showed that there were no cracks or pinholes and all the films were uniform and homogenous. While in H, H-AME and H-MME, SNP are absent, in H-SAME and H-SMME, SNP could be seen distributed throughout the matrix. The high-resolution images (Fig. 6c) of H-SAME and H-SMME distinctly exhibited the distribution of SNP as globules. In H-SMME, these SNP globules were homogenously distributed throughout the H matrix and were noticeably not agglomerated, thus indicating considerable homogeneity between the H matrix and SNP. However, smaller SNP globules were somewhat aggregated in H-SAME while the larger particles were apparently not agglomerated.

Unlike in H, H-AME and H-MME films (supporting file a,b,c), the presence of Ag-element was confirmed in H-SAME (10.02%) and H-SMME (12.57%) by elemental mapping (Akram et al., 2010; Alam et al., 2020).

3.4. TGA

The hydrogel films showed similar degradation pattern upto 150 °C (Fig. 7), which can be attributed to the loss of entrapped moisture. The next step incurred about 20 wt% loss upto 300°C in H, H-AME and H-MME, followed by the next step that extended

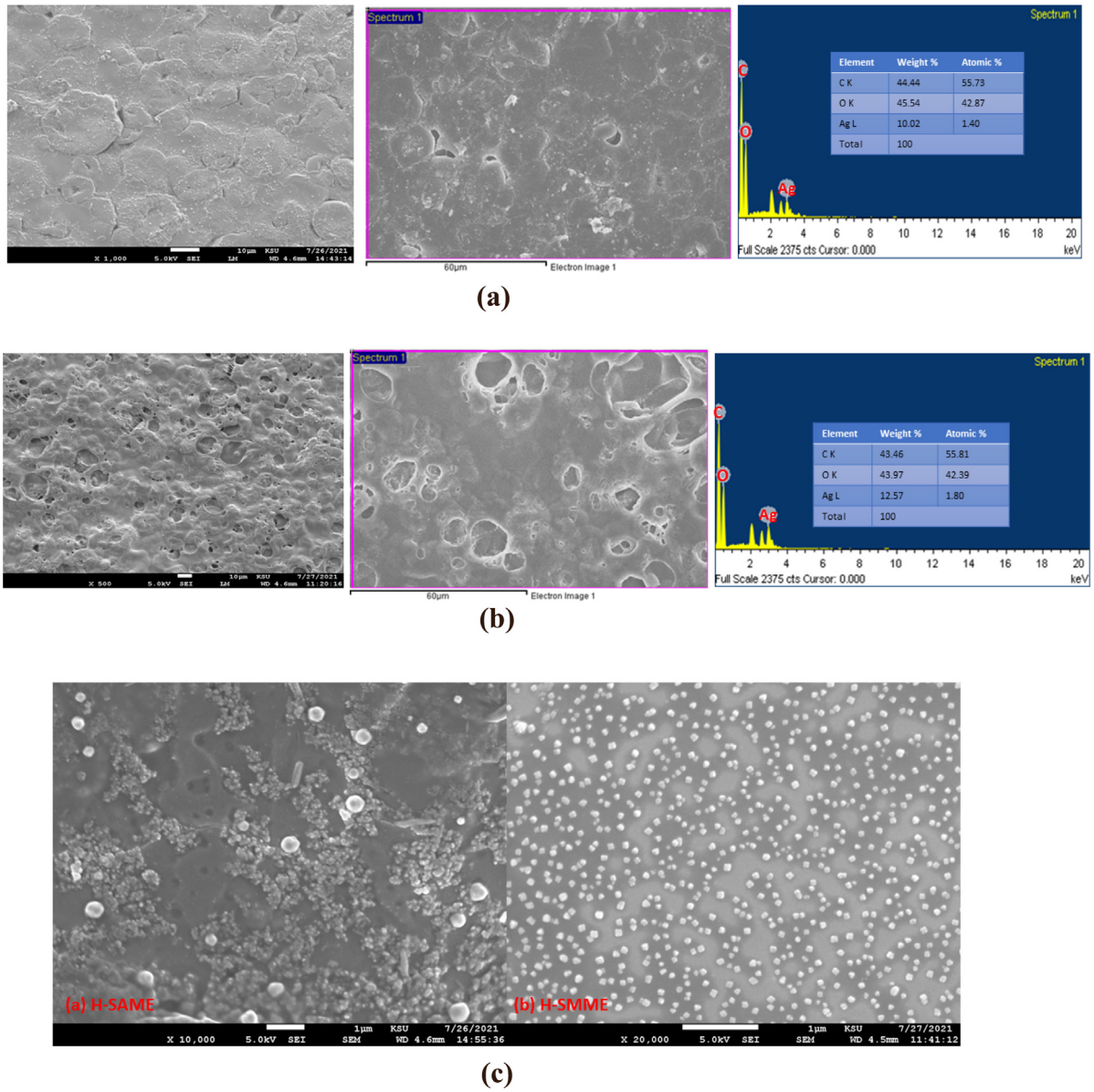

Fig. 6. (a) SEM of H-SAME. (b) SEM of H-SMME. (c) SEM of H-SAME and H-SMME (higher resolution).

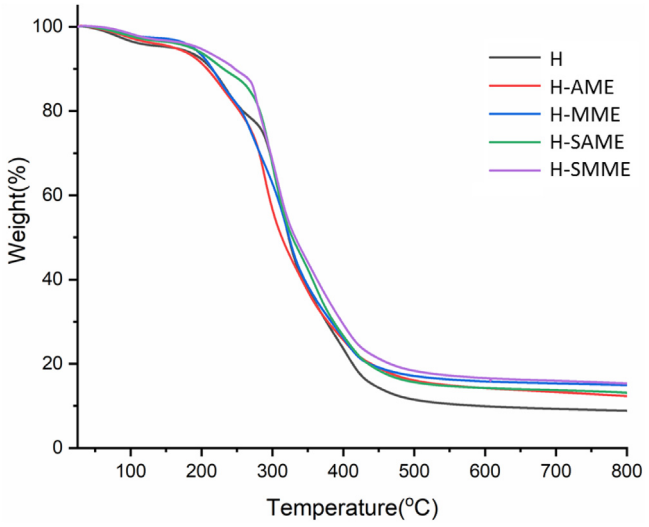

Fig. 7. TGA thermograms of H, H-AME, H-MME, H-SAME and H-SMME.

over the rest of the thermogram. In H, H-AME and H-MME, 10 wt% degradation occurred upto 210°C, while in H-SAME and H-SMME, the same occurred at 250°C and 260°C, respectively. In H, H-AME, H-MME, H-SAME and H-SMME, 50 wt% loss occurred in the range of 325°C–350°C, while 80 wt% loss occurred from 400°C to 415°C. The degradation pattern of H, H-AME and H-SAME was comparable. H-SMME showed higher thermal stability than H-SAME though both the hydrogel matrices were reinforced with SNP. This can be well explained with reference to the size of dispersed SNP and morphology of their respective hydrogel films (Fig. 6a and b). H-SMME has smaller size SNP homogenously dispersed throughout the matix while in H-SAME, SNP are relatively larger in size and clustered thus the homogeneity and integrity of the hydrogel matrix is expended.

Table 1
Antibacterial activity using disk diffusion method.

Mint extract preparation	Bacterial isolate	
	S. aureus (mm)	*P. aeruginosa* (mm)
AME	N/A	N/A
H-AME	N/A	N/A
SAME	7.7	7.5
H-SAME	8.33	9
MME	N/A	N/A
H-MME	N/A	N/A
SMME	7.33	9.5
H-SMME	8.33	9.5
CO	6.7	7
H	N/A	N/A
Amoxicillin	13.7	
Amikacin		19.7

3.5. Antibacterial study

Disk diffusion method using different samples (filter paper and hydrogel) showed different zones of inhibition as listed in Table 1. The zones of inhibition were measured in millimeters (mm). The positive control (Amoxicillin) for *S. aureus* showed 13.7 mm zone of inhibition. H-SAME showed zone of inhibition for *S. aureus* (8.33 mm) while SAME showed medium effect (7.7 mm). CO exhibited the lowest inhibition (6.7 mm). Similarly, addition of $AgNO_3$ to aqueous mint extract and methanolic mint extract hydrogel films showed medium zone of inhibition (9 and 9.5) in comparison to the positive control (Amikacin) which was 19.7 mm for *P. aeruginosa.* H, H-AME and H-MME films showed no effect on both *S. aureus* and *P. aeruginosa.* It is obvious that the addition of $AgNO_3$ to the aqueous mint extract and methanolic mint extract, followed by the synthesis of SNP, increased the effect of inhibiting the growth of both *S. aureus* and *P. aeruginosa* by hydrogel films.

Our extended studies demonstrated that the PVA:CS:CO hydrogel films loaded with SNP, showed potential for wound healing because of the dispersion of nanosized SNP.

3.6. Soil burial degradation

The hydrogel films were buried under soil and observed for any change in color, texture, weight and overall appearance of the films, after every 4 days. The signs of degradation became prominent after 12 days of soil burial. The films turned soft and became very fragile. H, H-AME and H-MME films had turned so weak that they could not be handled and they broke. This can be correlated to the presence of CO that aggravated degradation. H-SAME and H-SMME films had also turned very soft due to the absorption of water under the effect of soil, however, they did not break on handling and seemed to have retained their mechanical strength due to the presence of SNP. However, after 20 days of burial, both H-SAME and H-SMME films were degraded in pieces. The change in color was evident in all the films (Fig. 8). Thus, our study confirmed that all hydrogel films were biodegradable, therefore, after using the hydrogel films they can be easily degraded in soil.

4. Conclusion

PVA, CS and CO based hydrogel films were easily fabricated through simple, environment friendly, quicker route without any harmful solvents, arduous steps and side reactions. The hydrogel

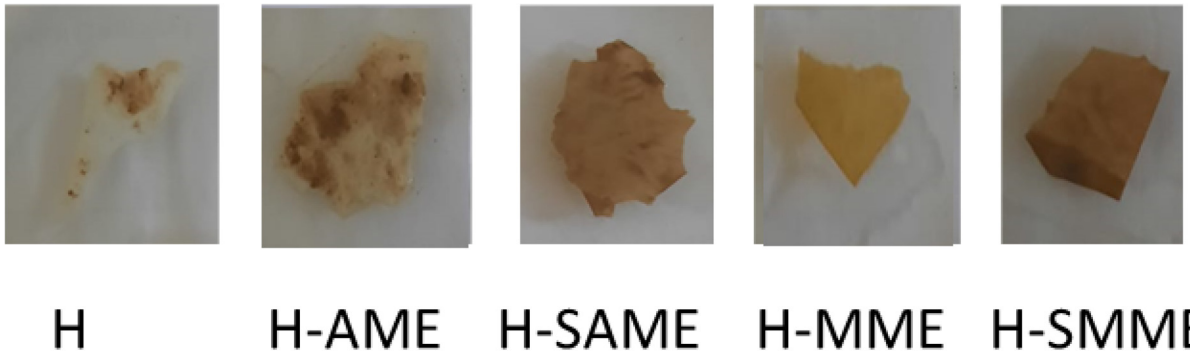

Fig. 8. Hydrogel films after soil biodegradation.

films were foldable, crackfree and thermally stable. They showed antibacterial activity against *S. aureus* and *P. aeruginosa*. The prepared films were found to be degradable in soil. These hydrogel films can be used as biodegradable and antibacterial wound dressings.

Funding

Funded by Deanship of Scientific Research at Umm Al-Qura University, Makkah, Saudi Arabia, by grant code: 19-MED-1-03-0008.

Declaration of Competing Interest

The authors declare that they have no known competing financial interests or personal relationships that could have appeared to influence the work reported in this paper.

Acknowledgements

The authors would like to thank the Deanship of Scientific Research at Umm Al-Qura University for the continuous support. This work was supported financially by the Deanship of Scientific Research at Umm Al-Qura University to Dr Mariam Mojally (Grant Code: 19-MED-1-03-0008).

The authors are thankful to Dr. Kadry Abdel Khalik, Botany Department, Faculty of Applied Sciences, Umm Al-Qura University for identification of the plant *Mentha piperita*.

Authors acknowledge with great appreciation the contribution of Mrs Deeba Aiman, Head of the Department & Lecturer (English), Boston World School, Pune, India, for English language corrections.

Authors appreciate the help rendered during experimental work by Mrs Afnan Abdulhamaid Hassan Sindi (Laboratory Technician, Pharmacy College, Umm Al-Qura University).

Authors are grateful to the College of Pharmacy for providing opportunity and facilities to carry out the research work.

References

Akram, D., Ahmad, S., Sharmin, E., Ahmad, S., 2010. Silica reinforced organic-inorganic hybrid polyurethane nanocomposites from sustainable resource. Macromol. Chem. Phys. 211 (4), 412–419. https://doi.org/10.1002/macp.200900404.

Akram, D., Sharmin, E., Ahmad, S., 2008. Synthesis, characterization and corrosion protective properties of boron-modified polyurethane from natural polyol. Prog. Org. Coat. 63 (1), 25–32. https://doi.org/10.1016/j.porgcoat.2008.04.003.

Aktürk, A., Erol Taygun, M., Karbancıoğlu Güler, F., Goller, G., Küçükbayrak, S., 2019. Fabrication of antibacterial polyvinylalcohol nanocomposite mats with soluble starch coated silver nanoparticles. Colloids Surf., A 562, 255–262. https://doi.org/10.1016/j.colsurfa.2018.11.034.

Alam, M., M Alandis, N., Sharmin, E., Ahmad, N., Husain, F.M., Khan, A., 2020. Mechanically strong, hydrophobic, antimicrobial, and corrosion protective polyesteramide nanocomposite coatings from leucaena leucocephala oil: a sustainable resource. ACS Omega 5 (47), 30383–30394. https://doi.org/10.1021/acsomega.0c03333.

Díez-Pascual, A.M., Díez-Vicente, A.L., 2015. Wound healing bionanocomposites based on castor oil polymeric films reinforced with chitosan-modified ZnO nanoparticles. Biomacromolecules 16 (9), 2631–2644. https://doi.org/10.1021/acs.biomac.5b00447.

Figueiredo, K.C.S., Alves, T.L.M., Borges, C.P., 2009. Poly(vinyl alcohol) films crosslinked by glutaraldehyde under mild conditions. J. Appl. Polym. Sci. 111 (6), 3074–3080. https://doi.org/10.1002/app.29263.

Gharibi, R., Shaker, A., Rezapour-Lactoee, A., Agarwal, S., 2021. Antibacterial and biocompatible hydrogel dressing based on gelatin- and castor-oil-derived biocidal agent. ACS Biomater. Sci. Eng. 7 (8), 3633–3647. https://doi.org/10.1021/acsbiomaterials.1c00706.

Ghosal, A., Iqbal, S., Ahmad, S., 2019. NiO nanofiller dispersed hybrid Soy epoxy anticorrosive coatings. Prog. Org. Coat. 133, 61–76. https://doi.org/10.1016/j.porgcoat.2019.04.029.

Ghosal, A., Rahman, O.U., Ahmad, S., 2015. High-performance soya polyurethane networked silica hybrid nanocomposite coatings. Ind. Eng. Chem. Res. 54 (51), 12770–12787. https://doi.org/10.1021/acs.iecr.5b02098.

Ghosal, A., Shah, J., Kotnala, R.K., Ahmad, S., 2013. Facile green synthesis of Nickel nanostructures using natural polyol and morphology dependent dye adsorption properties. J. Mater. Chem. A 1 (41), 12868.

Hassan, A., Niazi, M.B.K., Hussain, A., Farrukh, S., Ahmad, T., 2018. Development of anti-bacterial PVA/starch based hydrogel membrane for wound dressing. J. Polym. Environ. 26 (1), 235–243. https://doi.org/10.1007/s10924-017-0944-2.

Iqbal, D.N., Shafiq, S., Khan, S.M., Ibrahim, S.M., Abubshait, S.A., Nazir, A., Abbas, M., Iqbal, M., 2020. Novel chitosan/guar gum/PVA hydrogel: Preparation, characterization and antimicrobial activity evaluation. Int. J. Biol. Macromol. 164, 499–509. https://doi.org/10.1016/j.ijbiomac.2020.07.139.

Khan, N.A., Niazi, M.B.K., Sher, F., Jahan, Z., Noor, T., Azhar, O., Rashid, T., Iqbal, N., 2021. Metal organic frameworks derived sustainable polyvinyl alcohol/starch nanocomposite films as robust materials for packaging applications. Polymers 13 (14), 2307. https://doi.org/10.3390/polym13142307.

Khatoon, A., Khan, F., Ahmad, N., Shaikh, S., Rizvi, S.M.D., Shakil, S., Al-Qahtani, M.H., Abuzenadah, A.M., Tabrez, S., Ahmed, A.B.F., Alafnan, A., Islam, H., Iqbal, D., Dutta, R., 2018. Silver nanoparticles from leaf extract of Mentha piperita: eco-friendly synthesis and effect on acetylcholinesterase activity. Life Sci. 209, 430–434. https://doi.org/10.1016/j.lfs.2018.08.046.

Kouser, R., Vashist, A., Zafaryab, M., Rizvi, M.A., Ahmad, S., 2018a. Biocompatible and mechanically robust nanocomposite hydrogels for potential applications in tissue engineering. Mater. Sci. Eng., C 84, 168–179. https://doi.org/10.1016/j.msec.2017.11.018.

Kouser, R., Vashist, A., Zafaryab, M.d., Rizvi, M.A., Ahmad, S., 2018b. Na-montmorillonite-dispersed sustainable polymer nanocomposite hydrogel films for anticancer drug delivery. ACS Omega 3 (11), 15809–15820. https://doi.org/10.1021/acsomega.8b01691.

Kouser, R., Vashist, A., Zafaryab, M., Rizvi, M.A., Ahmad, S., 2018c. pH-responsive biocompatible nanocomposite hydrogels for therapeutic drug delivery. ACS Applied Bio Materials 1 (6), 1810–1822. https://doi.org/10.1021/acsabm.8b00260.

MubarakAli, D., Thajuddin N Fau - Jeganathan, K., Jeganathan K Fau - Gunasekaran, M., Gunasekaran, M. Plant extract mediated synthesis of silver and gold nanoparticles and its antibacterial activity against clinically isolated pathogens. (1873-4367 (Electronic)).

Muzammil, K.M., Mukherjee, D., Azamthulla, M., Teja, B.V., Kaamnoore, D., Anbu, J., Srinivasan, B., Jeevan Kasture, G., 2021. Castor oil reinforced polymer hybrids for skin tissue augmentation. Int. J. Polym. Mater. Polymeric Biomater. 70 (8), 530–544. https://doi.org/10.1080/00914037.2020.1740986.

Narayanan, K.B., Sakthivel, N., 2010. Biological synthesis of metal nanoparticles by microbes. Adv. Colloid Interface Sci. 156 (1–2), 1–13. https://doi.org/10.1016/j.cis.2010.02.001.

Narayanan, K.B., Sakthivel, N., 2011. Green synthesis of biogenic metal nanoparticles by terrestrial and aquatic phototrophic and heterotrophic eukaryotes and biocompatible agents. Adv. Colloid Interface Sci. 169 (2), 59–79. https://doi.org/10.1016/j.cis.2011.08.004.

Patil, M.P., Kim, G.-D., 2017. Eco-friendly approach for nanoparticles synthesis and mechanism behind antibacterial activity of silver and anticancer activity of gold nanoparticles. Appl. Microbiol. Biotechnol. 101 (1), 79–92. https://doi.org/10.1007/s00253-016-8012-8.

Rajeshkumar, S., Bharath, L. V. Mechanism of plant-mediated synthesis of silver nanoparticles – A review on biomolecules involved, characterisation and antibacterial activity. (1872-7786 (Electronic)).

Rezaei Hosseinabadi, S., Parsapour, A., Nouri Khorasani, S., Razavi, S.M., Hashemibeni, B., Heidari, F., Khalili, S., 2020. Wound dressing application of castor oil- and CAPA-based polyurethane membranes. Polym. Bull. 77 (6), 2945–2964. https://doi.org/10.1007/s00289-019-02891-z.

Robles-Martínez, M., Patiño-Herrera, R., Pérez-Vázquez, F.J., Montejano-Carrizales, J. M., González, J.F.C., Pérez, E., 2020. Mentha piperita as a natural support for silver nanoparticles: a new Anti- Candida albicans treatment. Colloid Interface Sci. Commun. 35, 100253. https://doi.org/10.1016/j.colcom.2020.100253.

Rosman, N.S.R., Harun, N.A., Idris, I., Ismail, W.I.W., 2020. Eco-friendly silver nanoparticles (AgNPs) fabricated by green synthesis using the crude extract of marine polychaete, Marphysa moribidii: biosynthesis, characterisation, and antibacterial applications. Heliyon 6 (11), e05462. https://doi.org/10.1016/j.heliyon.2020.e05462.

Sharmin, E., Batubara, A.S., Tamboosi, B.A., Al Khozay, E.B., Alamoudi, M.K., Al Aidaroos, O.Z., Alam, M., 2021. PVA nanocomposite hydrogel loaded with silver nanoparticles enriched Nigella sativa oil. Inorganic Nano-Metal Chem. 1–9. https://doi.org/10.1080/24701556.2021.1963277.

Sharmin, E., Kafyah, M.T., Alzaydi, A.A., Fatani, A.A., Hazazzi, F.A., Babgi, S.K., Alqarhi, N.M., Sindi, A.A.H., Akram, D., Alam, M., Alam, J., Al-Madboly, L.A., Shoeib, N.A., Alqahtani, A.M., Mojally, M., 2020. Synthesis and characterization of polyvinyl alcohol/corn starch/linseed polyol-based hydrogel loaded with biosynthesized silver nanoparticles. Int. J. Biol. Macromol. 163, 2236–2247. https://doi.org/10.1016/j.ijbiomac.2020.09.044.

Siddeeg, A., Salih, Z., Mukhtar, R., & Ali, A. (2018). Extraction and Characterization of Peppermint (Mentha piperita) Essential Oil and its Assessment as Antioxidant and Antibacterial. *13*, 1–15.

Sin, L.T., Bee, S.-T., Tee, T.-T., Kadhum, A.A.H., Ma, C., Rahmat, A.R., Veerasamy, P., 2013. Characterization of α-tocopherol as interacting agent in polyvinyl alcohol–starch blends. Carbohydr. Polym. 98 (2), 1281–1287. https://doi.org/10.1016/j.carbpol.2013.07.069.

Tanwar, R., Gupta, V., Kumar, P., Kumar, A., Singh, S., Gaikwad, K.K., 2021. Development and characterization of PVA-starch incorporated with coconut shell extract and sepiolite clay as an antioxidant film for active food packaging

applications. Int. J. Biol. Macromol. 185, 451–461. https://doi.org/10.1016/j.ijbiomac.2021.06.179.
Vashist, A., Ghosal, A., Vashist, A., Kaushik, A., Gupta, Y.K., Nair, M., Ahmad, S., 2019. Impact of nanoclay on the pH-responsiveness and biodegradable behavior of biopolymer-based nanocomposite hydrogels. Gels (Basel, Switzerland) 5 (4), 44. https://doi.org/10.3390/gels5040044.
Vashist, A., Gupta, Y.K., Ahmad, S., 2012. Interpenetrating biopolymer network based hydrogels for an effective drug delivery system. Carbohydr. Polym. 87 (2), 1433–1439. https://doi.org/10.1016/j.carbpol.2011.09.030.
Vashist, A., Kaushik, A., Vashist, A., Jayant, R.D., Tomitaka, A., Ahmad, S., Gupta, Y.K., Nair, M., 2016. Recent trends on hydrogel based drug delivery systems for infectious diseases. Biomater. Sci. 4 (11), 1535–1553. https://doi.org/10.1039/C6BM00276E.
Vashist, A., Shahabuddin, S., Gupta, Y.K., Ahmad, S., 2013. Polyol induced interpenetrating networks: Chitosan-methylmethacrylate based biocompatible and pH responsive hydrogels for drug delivery system. J. Mater. Chem. B 1 (2), 168–178. https://doi.org/10.1039/C2TB00021K.
Vashist, A., Vashist, A., Gupta, Y.K., Ahmad, S., 2014. Recent advances in hydrogel based drug delivery systems for the human body. J. Mater. Chem. B 2 (2), 147–166. https://doi.org/10.1039/C3TB21016B.
Velgosova, O., Mudra, E., Vojtko, M., 2021. Preparing, characterization and anti-biofilm activity of polymer fibers doped by green synthesized AgNPs. Polymers 13 (4), 605. https://doi.org/10.3390/polym13040605.